ASME Journal of Fluids Engineering
Online journal at:
https://asmedigitalcollection.asme.org/fluidsengineering

Nathan P. Hagstrom
Department of Mechanical Engineering,
University of Minnesota,
111 Church St. SE,
Minneapolis, MN 55414
e-mail: hagst082@umn.edu

Matthew L. Gallagher
Department of Mechanical Engineering,
University of Minnesota,
111 Church St. SE,
Minneapolis, MN 55455
e-mail: galla418@umn.edu

Thomas R. Chase[1]
Fellow ASME
Department of Mechanical Engineering,
University of Minnesota,
111 Church St. SE,
Minneapolis, MN 55455
e-mail: trchase@umn.edu

Compressible Flow Through Flat Valve Seals at Microscale Displacements

Existing analytical flow models for predicting flow rates at microscale seal displacements are limited to two separate domains. The first assumes a small channel length to height aspect ratio at relatively large seal displacements. The second assumes a large channel length to height aspect ratio at relatively small seal displacements. A piecewise analytical model for compressible flow is developed here to enable predicting flow rates in valves with fluid pathways of any aspect ratio. The new model is validated by numerical studies and experiment. The results are applicable to flat valve seals having a cylindrical seal boss feature with fluid passage length to height aspect ratios ranging from 3.3 to 800. The new model is particularly useful for the design of microvalves and macroscale valves with small actuator displacements. [DOI: 10.1115/1.4065383]

Keywords: compressible flow, flow modeling, flow control, valve

1 Introduction

Microvalves have been a subject of academic research for decades due to their diminutive size, light weight, energy efficiency, and ability to precisely control small amounts of flow [1]. Microvalves generally contain three fundamental components: an actuator, a seal, and an orifice. Within the scope of this work, a microvalve is defined as a valve with transport rates and characteristic flow passage dimensions on the microscale. Characteristic flow passage dimensions include displacement between the seal and the orifice, seal diameter, and orifice diameter. In most microvalves, actuator displacement is sized to be much smaller than the orifice diameter to enforce seal limited flow, limiting total actuator displacement to tens of micrometers [1].

Given the small length scale of microvalve flow passage characteristic dimensions, use is often limited to gaseous media. Microvalve use can be extended to systems using liquids so long as small flow capacities are acceptable. Applications that stand to benefit from microvalve use include micropropulsion, aerospace fluid control systems, biological diagnostic systems, mobile robotics, refrigeration coolant management, and precision gas control.

Recent academic research on microvalve design has focused on a few key areas including methods for reducing leakage, methods for increasing flow capacity, and flow modeling at small actuator displacements. Improved parametric understanding of compressible flow through valve seals can help further inform methods for reducing leakage and increasing flow capacity. The relevant literature is reviewed in Sec. 1.1.

1.1 Background. A seal in the context of this work comprises a seal plate sealing against an orifice plate. Seal plates commonly take one of two forms: a simple flat plate or a flat plate with a cylindrical boss. The face of the seal or the seal boss that makes contact with the orifice plate is described as a seal seat. An orifice plate is defined as any flat structure containing an orifice. The region on the orifice plate where the seal makes contact is defined as the valve seat.

Methods for reducing leakage focus primarily on seal design or valve seat design. Research to improve sealing in microvalves has centered on two areas, use of deformable valve seats [2–4] and rigid valve seats [5–11], with the majority of work taking place on the latter.

Efforts to improve flow capacity in valves with microscale actuator displacements have focused on valve seat design, orifice design, and actuator sizing. Wijngaart et al. [9] present data and a model used to optimize the ratio of the orifice diameter relative to the length of the valve seat perimeter. They also present a piecewise flow model that describes a transition between the seal-limited flow regime and the orifice-limited flow regime. The result enables minimizing actuator stroke for a given target flowrate.

Existing flow models for microvalves generally fit into two categories. The first predicts flow rates in the seal-limited flow regime by modification of the traditional orifice flow equations (for example, White [12]). Henning developed a piecewise flow model that describes flowrate as a function of valve seal displacement where the flow regime moves from seal-limited flow, to a transition regime, and finally to the orifice-limited regime [13–15]. Henning's model assumed linear flow as a function of displacement for the

[1]Corresponding author.

Contributed by the Fluids Engineering Division of ASME for publication in the Journal of Fluids Engineering. Manuscript received September 30, 2023; final manuscript received March 31, 2024; published online May 24, 2024. Assoc. Editor: Shanti Bhushan.

entire range of seal-limited flow. An empirical relationship between flowrate and the restricting area is developed. Wijngaart et al. presented similar empirical evidence to Henning.

The second category focuses on understanding the flowrate characteristics of valve seals at very small displacements. Pan and Wang [11] designed a microvalve to control liquid flow using a disk type piezo bender. They developed a Bernoulli equation-based analytical flow model to predict flow rates in microvalves at seal displacements up to 30 μm. Johnson et al. [7] designed a piezoelectric stack (piezostack)-controlled microvalve with an etched silicon valve seat using concentric rings. They also developed a one-dimensional model for frictional flow through the valve at small seal displacements. The primary contribution was defining an empirically based friction coefficient dependent on the Reynolds number of the flow.

Microchannel flow has been widely studied due to extensive applications and as a result, the physics are well understood [16–20]. A microchannel flow model developed by Arkilic was created through direct solution of the two-dimensional compressible Navier–Stokes equations [16]. This model accounts for wall slip at small channel heights as well as for compressibility effects. At microscale valve seal displacements, seal-limited flow has been modeled as equivalent to microchannel flow [5].

1.2 Motivation. Limitations of existing flow models inhibit the ability of engineers to employ model-based valve design. Existing models are limited to either a microchannel-based model or a seal-limited flow model based on orifice flow theory. The flow modeling approach described in this work expands on previous models by hybridizing the microchannel-based approach with the seal-limited approach. The result enables modeling valves having flow regimes that move between the microchannel regime at small displacements and the seal-limited regime at larger displacements.

The aforementioned models are compared to the model produced in this work in Fig. 1. Experimental data points from an actual valve having a 30-μm actuator displacement, described in Sec. 5, is overlaid on the analytical curves. The existing channel flow model works well for about the first 7 μm of displacement but becomes unusable for larger displacements. The existing orifice flow model works poorly for low displacements and exhibits a substantial offset error for higher displacements. The piecewise flow model, developed in Sec. 3, represents actual flow data accurately throughout the range of travel.

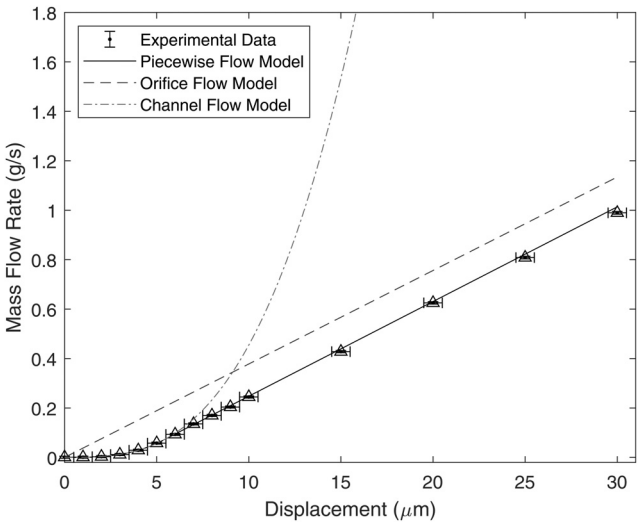

Fig. 1 Comparison between orifice (linear) flow models [9,13], channel (cubic) flow models [5,20], and the model developed in Sec. 3 for a seal plate with $t_s = 654$ μm at 600 kPa gauge inlet pressure. Experimental data from an actual valve with 30 μm of travel, described in Sec. 5, is overlaid on the analytical curves. The piecewise flow model developed in Sec. 3 produces accurate predictions for flow throughout the range of valve travel.

The new model enables designing efficient seal plates compatible with microscale actuation strategies such as piezo-electric, electrostatic, magnetic, thermal, and any other actuation strategy that operates with seal plate displacements of the order of tens to hundreds of micrometers. Piezo-electric stack (piezostack) actuators are of particular interest due to their low power consumption, fast response time, and high output force.

Section 2 describes the design and fabrication of the valve seal. The piecewise analytical flow model represented in Fig. 1 is developed (Sec. 3) and then validated both numerically (Sec. 4) and experimentally (Sec. 5). In addition, the effect of seal geometry on the range of controllable flow (Sec. 4.2) and leak rate (Sec. 5.3) is explored. The significance of the new model is discussed in Sec. 6. Section 7 concludes the paper.

2 Valve Seal Design

The design objectives for the valve seals utilized in the experiments were threefold. The first was to achieve low leak rates. The second was to enable increased flow capacity in valves using actuators with microscale displacements. The third was to use a rigid valve seal, as opposed to an elastomeric seal, to enable compatibility with clean processes such as bioreactors and microfabrication processes.

The flow models developed in this work apply to flat seals and flat seals with seal boss features. The seals used in the experimental test bed include a seal boss (see Fig. 2). The boss seals against an orifice plate. The boss increases sealing pressure, which reduces leak rates. In addition, it enables increasing flow capacity through the seal assembly, as described in Sec. 4.2.

Referencing Fig. 2, δ is the displacement of the seal plate from the orifice plate, h_s is the height of the seal boss, t_s is the radial width of the seal boss, h_p is the thickness of the seal plate following etching, D_s is the inner diameter of the seal boss, and D_o is the orifice diameter. The dashed lines represent section views of two cylindrical areas of interest, described here as "peripheral areas." Design parameters held constant in this study were $h_s = 152.5$ μm and $D_o = 2780$ μm.

The peripheral area created by the seal boss ($A_{s,\text{periph}} = \pi D_s \delta$) is characterized by the outermost dashed line in Fig. 2. Similarly, the peripheral area created by the orifice ($A_{o,\text{periph}} = \pi D_o(\delta + h_s)$) is characterized by the innermost dashed line. The final area of interest is the cross-sectional area of the orifice ($A_o = \pi D_o^2/4$). The seal plate is designed in such a way that $A_{s,\text{periph}}$ is the restricting flow area over the intended range of operation of the seal plate.

A prototype valve was constructed to perform the experiments. The seal plate was fabricated out of annealed 305-μm thick 303 stainless steel using photochemical etching (PCE). Annealed

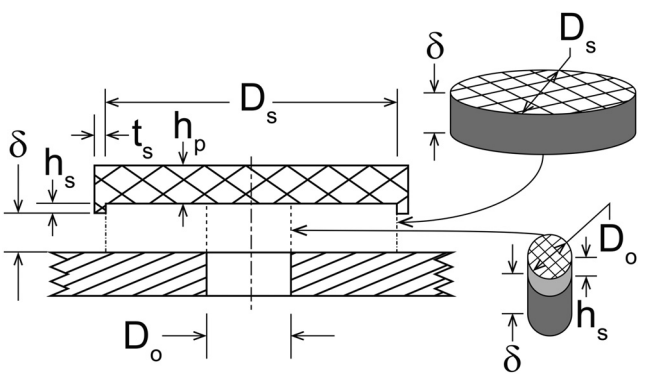

Fig. 2 Parameterized cross-sectional view of the seal plate with a seal boss (top) displaced a distance from an orifice plate (bottom)

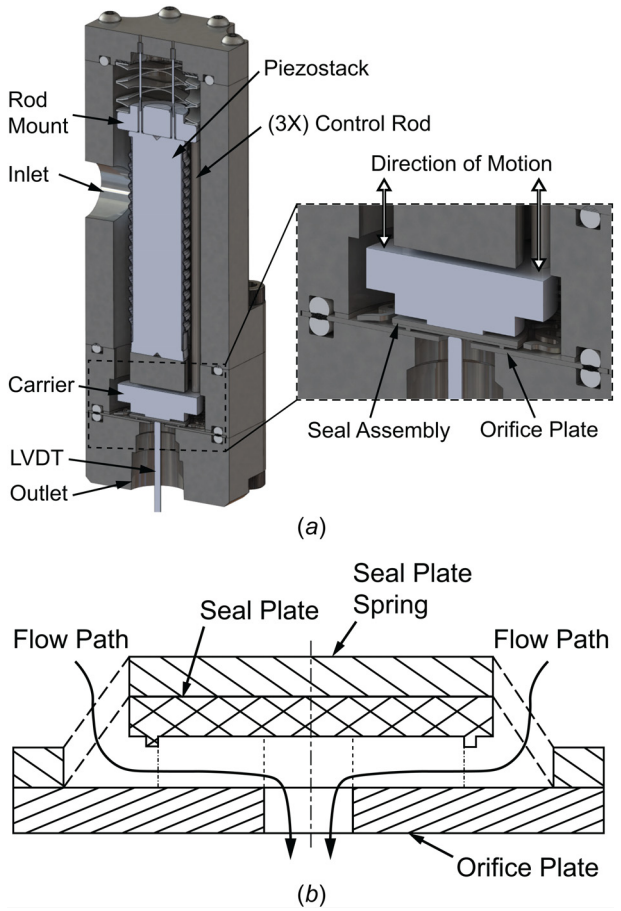

Fig. 3 Prototype valve design and flow pathways: (*a*) cross sections of prototype valve assembly and (*b*) schematic of the flow path through a valve seal assembly mounted against an orifice

material was used to minimize distortion as a result of PCE. Post-PCE, the seal seat and the orifice plate were lapped to a mirror finish.

A cross section of the prototype valve is shown in Fig. 3(*a*). The seal position is controlled by a piezostack actuator.[2] The bottom of the piezostack is mounted to a stationary base, which is rigidly connected to the exterior housing.

The top of the piezostack translates vertically. A rod mount is attached to the top of the piezostack. Three vertical control rods are connected to the rod mount. The rods are positioned radially outside of the piezostack and pass through holes in the stationary base.

The seal plate carrier is connected to the bottom end of the control rods. The seal plate is pressed against the orifice plate by springs (one of which is visible in Fig. 3(*b*)) when the piezostack is unpowered. The piezostack expands when powered, lifting the rod mount, the control rods, and the seal plate away from the orifice plate. This architecture enables keeping the brittle piezostack in compression in a normally closed valve design. Furthermore, the thermal expansion properties of the piezostack and the control rods can be matched to minimize changes in performance due to changes in temperature.

3 Piecewise Analytical Flow Model

Flow through a seal with a seal boss at very small displacements can be described by drawing parallels to flow through rectangular smooth microchannels. Arkilic et al. [16] developed a model for mass flow through high aspect ratio rectangular microchannels that compensates for compressibility effects and accommodates rarefied gas effects leading to nonzero tangential velocity at the microchannel walls

[2]Physik Instrumente P-885.95.

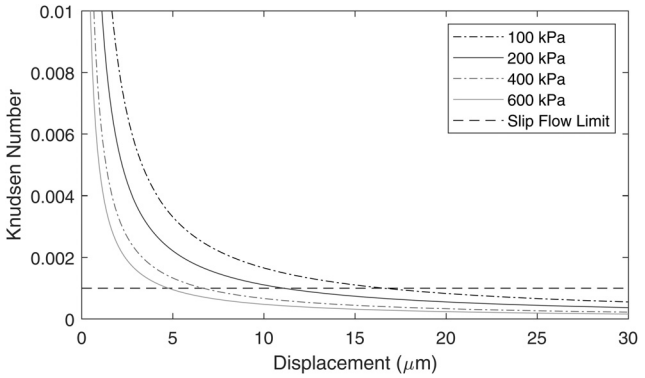

Fig. 4 K_n plotted against seal displacement at varying inlet pressures. Pressures shown are gauge pressures.

$$\dot{m} = \frac{H^3 w {P_2}^2}{24\mu LRT}\left(\left(\frac{P_1}{P_2}\right)^2 - 1 + 12\sigma K_n\left(\frac{P_1}{P_2} - 1\right)\right) \tag{1}$$

where H is the channel height in m, w is the channel width in m, P_1 is the absolute inlet pressure in Pa, P_2 is the absolute outlet pressure in Pa, μ is the dynamic viscosity in Pa·s, L is the channel length in m, R is the specific gas constant in J·kg/K, T_1 is the inlet temperature in K, σ is the stream-wise momentum accommodation coefficient, and K_n is the Knudsen number [12,21] for a microchannel

$$K_n = \frac{\mu(\pi D_s + \delta)}{D_s \delta P_1}\sqrt{\frac{\pi R T_1}{8}} \tag{2}$$

σ and K_n account for rarefied gas flows at wall boundaries.

For the seal plate designs studied, K_n is modeled in Fig. 4 alongside the slip flow limit of $K_n = 0.001$. In cases where $0.001 < K_n < 0.1$, flow is in a regime where slip or rarefication effects may be present. In cases where $K_n < 0.001$, it can be assumed that only compressibility effects are present and rarefied gas effects are absent [17]. When the seal displacement falls below 5 μm, rarefication effects may exist at all studied pressures. However, to simplify the microchannel model and following derivation, the Knutson term in Eq. (1) is assumed to be negligible,[3] simplifying (1) to

$$\dot{m} = \frac{H^3 w {P_2}^2}{24\mu LRT_1}\left(\left(\frac{P_1}{P_2}\right)^2 - 1\right) \tag{3}$$

Geometric parameters are converted from a rectangular microchannel to an annular microchannel by substituting πD_s for w, δ for H, and t_s for L in Eq. (3). A discharge coefficient, C_D, is then introduced to account for frictional effects

$$\dot{m} = C_a C_D\left(\frac{\pi\delta^3 D_S}{t_s}\right)\left({P_1}^2 - {P_2}^2\right) \tag{4}$$

where

$$C_a = \frac{1}{24\mu RT_1} \tag{5}$$

Flow described by Eq. (4) is defined as being in the microchannel flow regime.

Flow at larger displacements is classified as being in the seal limited flow regime. If $P_1 \geq 1.89\,P_2$, the flow is choked and therefore defined by the well-known equation [12]

[3]The reasonableness of ignoring the Knutson term in Eq. (1) is explored in Sec. 6.

$$\dot{m} = C_D C_b \pi D_s \delta P_1 \tag{6}$$

where

$$C_b = \sqrt{\frac{\gamma}{RT_1}\left(\frac{2}{1+\gamma}\right)^{\frac{\gamma+1}{\gamma-1}}} \tag{7}$$

γ is the ratio of specific heats and $\pi D_s \delta$ is the peripheral area created by the seal boss (see Fig. 2). The same discharge coefficient, C_D, is used as in the microchannel flow regime. Note that flow will vary linearly with displacement in the seal-limited regime if the input pressure remains constant.

The transition displacement, δ_T, is the displacement where the microchannel flow model described by Eq. (4) transitions into the seal limited flow model described by Eq. (6). In other words, if the valve seal is steadily displaced from the closed state, and $P_1 \geq 1.89\,P_2$, the flow chokes when δ_T is reached. δ_T is determined by locating the displacement where the slope of the microchannel flow model is equal to the slope of the seal-limited flow model

$$\delta_T = \sqrt{\frac{t_s P_1 C_b}{3\left(P_1^2 - P_2^2\right) C_a}} \tag{8}$$

An offset constant

$$\Delta\dot{m}_{\delta=\delta_T} = C_D \pi \delta_T D_s \left(\frac{{\delta_T}^2}{t_s}\left({P_1}^2 - {P_2}^2\right) C_a - P_1 C_b\right) \tag{9}$$

is defined to match the mass flowrate of the microchannel and seal-limited flow models at $\delta = \delta_T$. The final piecewise analytical flow model describing flowrate through a flat valve seal at both small and large displacements is

$$\dot{m} = \begin{cases} C_D\left(\dfrac{\pi\delta^3 D_S}{t_s}\right)\left({P_1}^2 - {P_2}^2\right) C_a & \delta < \delta_T \\ C_D C_b \pi \delta D_s P_1 + \Delta\dot{m}_{\delta=\delta_T} & \delta \geq \delta_T \end{cases} \tag{10}$$

Note that Eq. (10) is valid only if $P_1 \geq 1.89\,P_2$.

The discharge coefficient, C_D, is used to calibrate the model to experimental or numerical flow data. Calibration is most easily accomplished by plotting mass flowrate versus displacement data for a constant input pressure, P_1. A simple line is fit through the data points where the displacement exceeds δ_T (Eq. (8)). Then the slope of that line, $d\dot{m}/d\delta$, is measured. If input pressure, P_1, and temperature, T_1, are held constant, C_D can be found by taking the derivative of Eq. (6) with respect to δ

$$C_D = \frac{(d\dot{m}/d\delta)}{\pi D_S P_1 C_b} \tag{11}$$

The curve fits shown in Fig. 1 and Sec. 5 were performed in this manner.

An alternative means for calibrating the model is to determine the value of C_D that produces the best least-squares fit of Eq. (10) to all available data points at each individual pressure, including the data in the microchannel flow regime, then averaging the resulting C_D's. The alternative means was used to fit the analytical curves shown in Sec. 4.

4 Numerical Flow Modeling

Steady-state flow through the valve seal was numerically simulated using computational fluid dynamics (CFD). The mesh used to represent the prototype valve is described first. The model is then applied to estimate the controllable flow range of the prototype valve. The flow versus displacement behavior of the valve is then predicted with the numerical model and compared with the analytical model developed in Sec. 3.

4.1 Numerical Domain. The two-dimensional axisymmetric domain used to model flow through the prototype valve is shown in Fig. 5. The large volume upstream of the seal plate present in the prototype was ignored, as the velocity and related viscous flow losses in those regions were assumed to be insignificant. The volume downstream from the seal plate is captured in the mesh. Points 1 and 2 indicate the surfaces where the inlet and outlet boundary conditions are applied. The dot-dashed line in Fig. 5 is the axis of symmetry. All other surfaces were treated as walls with no-slip boundary conditions.

Meshing and simulation were performed using ANSYS FLUENT Academic Research Version 20.2. The transition shear stress transport (SST) turbulence model [22] was used. This model accurately represents the supersonic flow and corresponding shock structures present at the inner diameter of the seal boss. Previous literature found that this model accurately recreated supersonic shock structures present in free jets, which this model closely mirrors [23]. The transition SST model is also able to better model the transition between laminar and turbulent flow than the $k-\omega$ SST model as it adds two transport equations.

Unstructured grids were used to mesh the geometry shown on the left-hand side of Fig. 5 with the resulting mesh shown on the right-hand side. The unstructured grids were based off of prism layer meshes utilizing quadrilateral cells at the walls. Cell sizes at the walls were varied to maintain a y^+ value of less than one to ensure that the model was able to accurately resolve into the viscous sublayer. For example, 0.1-μm high cells were used at the surfaces of the seal plate boss with a 10% growth rate extending from the walls. A cell height of 0.4 μm, with an 11% growth rate, was used at the top of the orifice plate and the remaining surfaces of the seal plate. The

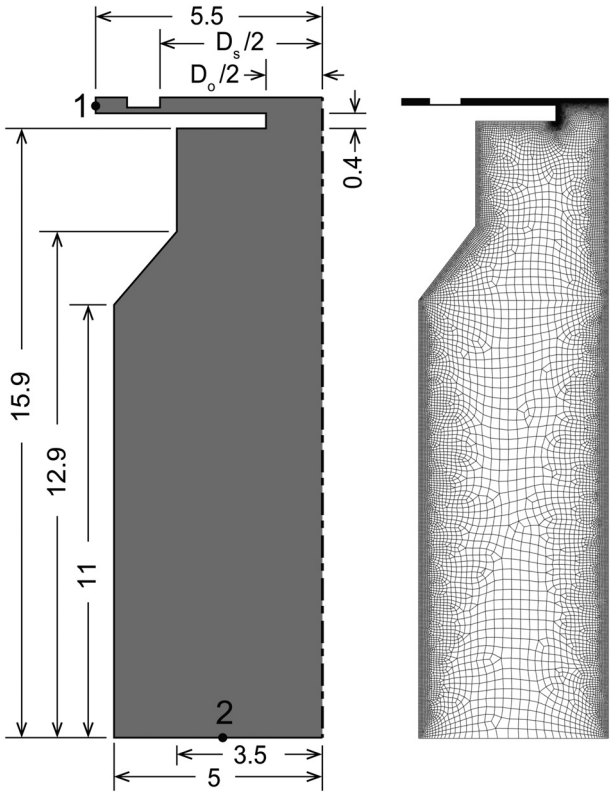

Fig. 5 Axisymmetric geometry modeled in CFD simulations with dimensions in units of mm

less critical downstream surfaces used a starting cell height of 30 μm with an 11% growth rate.

Special measures were taken for the 1-μm gap between the bottom of the seal plate boss and the top of the orifice plate for the minimum flowrate study: 0.1-μm high cells were used for the entirety of the gap.

Mesh sensitivity studies were performed at 600-kPa gauge inlet pressure. The heights of the cells at the walls, which drove the resolution of the remainder of the grid, were decreased progressively until the mass flowrate varied less than 1% from the previously tested grid. For example, the cells having a final height of 0.1 μm were reduced in the sequence {0.4 μm, 0.3 μm, 0.2 μm, 0.15 μm, and 0.1 μm}.

4.2 Controllable Flow Range Study. Relative minimum and maximum flow rates were studied as a function of seal boss width and height. The minimum flowrate, essentially modeling the leak rate, was studied by specifying $\delta = 1$ μm, as reducing δ further resulted in issues with model convergence due to low transport rates. Maximum flowrate was assessed at $\delta = 30$ μm, as this correlates with nominal strokes achievable by commercially available piezo-stack actuators. Design parameters held constant were $D_s = 7.80$ mm and $D_o = 2.78$ mm. Outlet pressure was set at 101.3 kPa, and stagnation temperature was assumed to be 294 K.

The leak rate was studied solely as a function of the seal boss width, as seal boss height was assumed to have a negligible impact on leak rate. The leak rates, estimated using the numerical model and the piecewise analytical model (Eq. (10)), are shown in Fig. 6. The numerical data and the piecewise analytical model generally agree, with better agreement at lower pressures and larger seal boss widths. Leak rates decreased as seal boss width increased. Leak rates as low as 4.74×10^{-4} g/s and 3.61×10^{-4} g/s were estimated using the numerical and analytical methods respectively with a seal boss width of 800 μm at 600 kPa gauge inlet pressure.

Mach number contours for the 800-μm wide seal boss at 600 kPa gauge inlet pressure and $\delta = 1$ μm are shown in Fig. 7. A largely developed channel-type velocity distribution [5] is revealed, with subsonic flow at the inner diameter of the seal boss and edge effects dominating the velocity field. At lower pressures, the flow was more developed than at higher pressures, explaining why the numerical values deviated from the analytical solutions more at higher pressures.

Mass flowrate is plotted as a function of seal boss width at $\delta = 30$ μm (maximum displacement) in Fig. 8. As with $\delta = 1$ μm, better analytical model agreement was observed with decreases in inlet pressure and with increases in seal boss width. The range of flow passage aspect ratios studied was from 3.3 to 26.7.

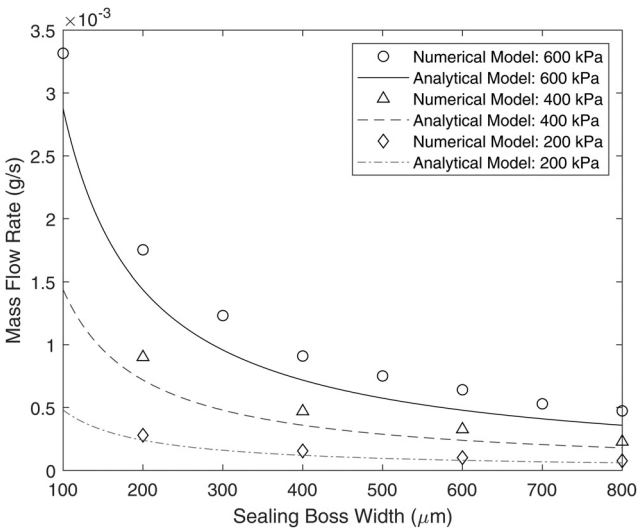

Fig. 6 Numerical model calculations for flowrate through etched metallic seals with seal bosses of varying width at $\delta = 1$ μm. $h_s = 152.5$ μm (Fig. 2). Predictions from the analytical model of Sec. 3 are overlaid. Pressures shown are gauge pressures.

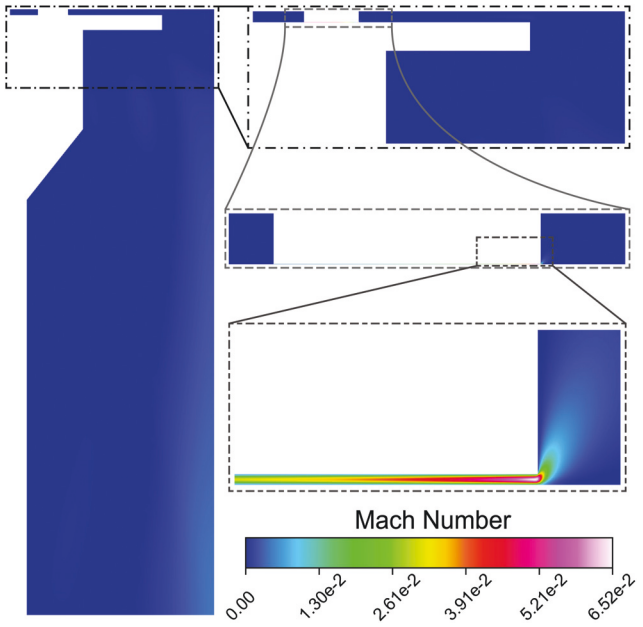

Fig. 7 Numerical Mach number gradient estimations for flow through an etched metallic seal plate with seal boss width of 800 μm and $h_s = 152.5$ μm at $\delta = 1$ μm and 600-kPa gauge inlet pressure

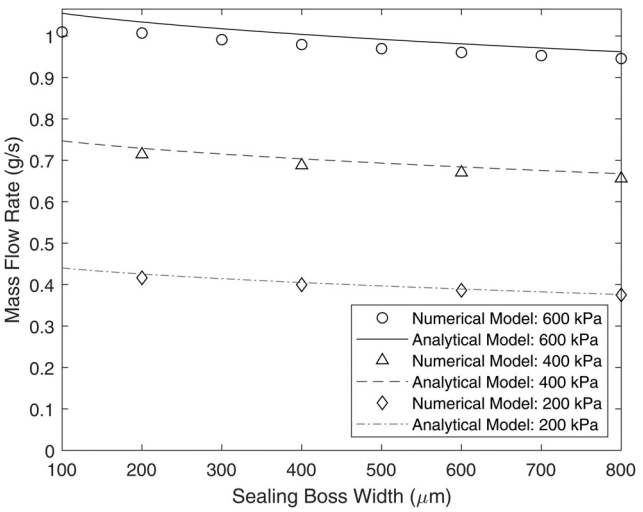

Fig. 8 Numerical model calculations for flowrate through etched metallic seals with seal bosses of varying width compared with the analytical model at $\delta = 30$ μm. $h_s = 152.5$ μm. Pressures shown are gauge pressures.

At 600-kPa gauge inlet pressure and a seal boss width of 800 μm, mass flowrates of 9.62×10^{-1} g/s and 9.46×10^{-1} g/s were estimated using the numerical and analytical methods, respectively. The numerically modeled leak rate and the maximum flowrate define a controllable flow range between 4.74×10^{-4} g/s and 9.46×10^{-1} g/s. This span yields a turndown ratio of 2000.[4]

Study of Mach number contours with $\delta = 30$ μm and inlet pressure at 600 kPa gauge (Fig. 9) revealed two regions of flow. The first is a region of subsonic flow between the seal boss and the orifice plate,

[4]A turndown ratio is the ratio of the maximum to the minimum controllable flow rate at a pressure.

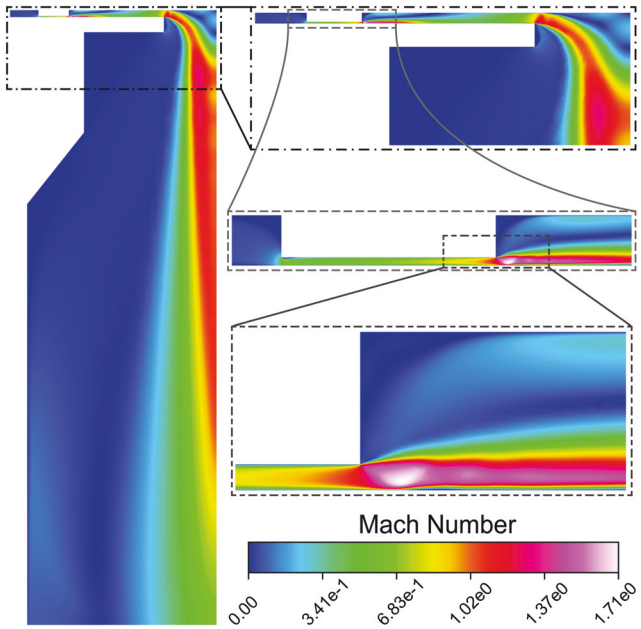

Fig. 9 Numerical Mach number gradient calculations for flow through an etched metallic seal plate with seal boss width of 800 μm and h_s= 152.5 μm at $\delta = 30\,\mu$m and 600-kPa gauge inlet pressure

and the second is a supersonic jet created at the outlet of the seal boss. Mild shocks are observable within the jet structure. These shocks were not observed at 400-kPa or 200-kPa gauge inlet pressures. Formation of the observed shock structures correlates with expected behavior from orifice-type flow.

The height at which the seal boss acted as the governing flow restriction, rather than the peripheral area above the orifice, is explored for an 800-μm wide seal boss in Fig. 10. Mass flowrate is plotted as function of the area ratio

$$A_{\text{ratio}} = \frac{D_o(\delta + h_s)}{D_s(\delta)} = \frac{A_{o,\text{periph}}}{A_{s,\text{periph}}} \tag{12}$$

Increasing the seal boss height from 0 μm to 200 μm provided increases in flow capacity with diminishing returns once $A_{\text{ratio}} > 1.54$.

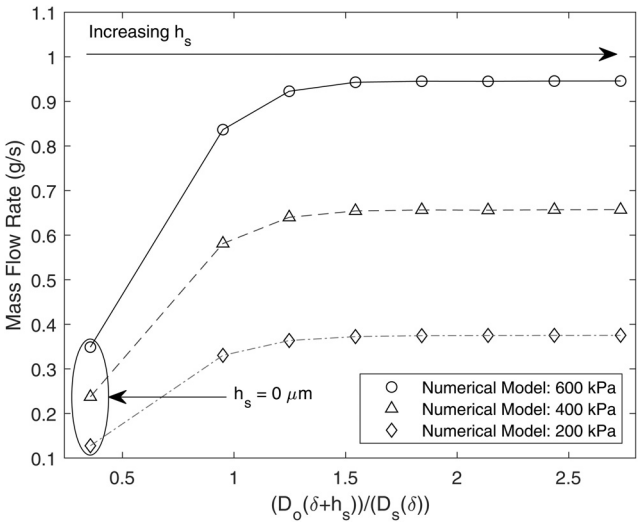

Fig. 10 Numerical model calculations for flowrate through etched metallic seals with $t_s = 800\,\mu$m, varying h_s and $\delta = 30\,\mu$m. ($h_s = 0$ and h_s=50−200 μm in increments of 50 μm.) Pressures shown are gauge pressures.

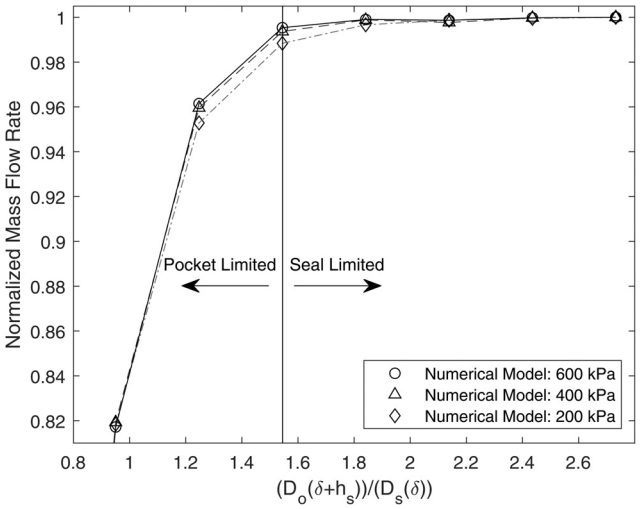

Fig. 11 Numerically calculated normalized flow capacity plotted against A_{ratio} to identify location of shift in flow regime. Pressures shown are gauge pressures.

To further illustrate this point, the flowrate data were normalized from 0 to 1 by

$$\dot{m}_{\text{norm},i} = \frac{\dot{m}_i - \min(\dot{m})}{\max(\dot{m}) - \min(\dot{m})} \tag{13}$$

(see Fig. 11). A transition between pocket limited flow and seal limited flow arises as h_s increases. $A_{\text{ratio}} = 1.54$ represents the location where the normalized mass flowrate is within 1% of its maximum value. When $A_{\text{ratio}} < 1.54$, the pocket created by the seal boss acts as the governing flow restriction. When $A_{\text{ratio}} > 1.54$, the seal boss acts as the governing flow restriction. To ensure the seal acts as the primary flow restriction and by extension, follows the piecewise analytical model, the seal boss and orifice should be designed such that $A_{\text{ratio}} > 1.54$. Smaller ratios may result in inconsistent control and reduced flow capacity.

In summary, the results of the piecewise analytical model closely matched those of the numerical model at both $\delta = 1\,\mu$m and $\delta = 30\,\mu$m. Seal boss width theoretically has a larger relative impact on leak rate in comparison to overall flow capacity. At 1-μm seal displacement, flow was found to be in the microchannel regime and subsonic at the outlet of the microchannel created by the seal boss. The flow model fit well in the seal-limited flow regime at 30-μm valve seal displacement with supersonic flow at all modeled pressures, and shocks created at 600-kPa gauge inlet pressure. To enable the maximum flow capacity from a seal plate in the seal-limited regime, the peripheral area above the orifice must be at least 54% larger than the peripheral area below the seal boss inner diameter. This ratio prevents flow restriction due to formation of a secondary region of choked flow near the peripheral area above the orifice.

4.3 Flow Rate Versus Displacement: Numerical. Flow rate versus displacement for a seal plate with $t_s = 800\,\mu$m is shown in Fig. 12. The discrete points represent CFD results while the continuous curves were generated using Eq. (10). A discharge coefficient of 0.91 was determined using the "alternative method" of model calibration described in Sec. 3. The piecewise analytical model closely matched numerical data with minutely increasing variation between models as pressure increases from 200- to 600-kPa gauge inlet pressure.

A closer view of the modeling results for the first 10 μm of displacement is shown in Fig. 13. The displacement where the microchannel model transitions to the seal-limited flow model, δ_T, is plotted as a dotted line for each pressure. Trends in the numerical data agreed with Eq. (8), showing pressure difference having a

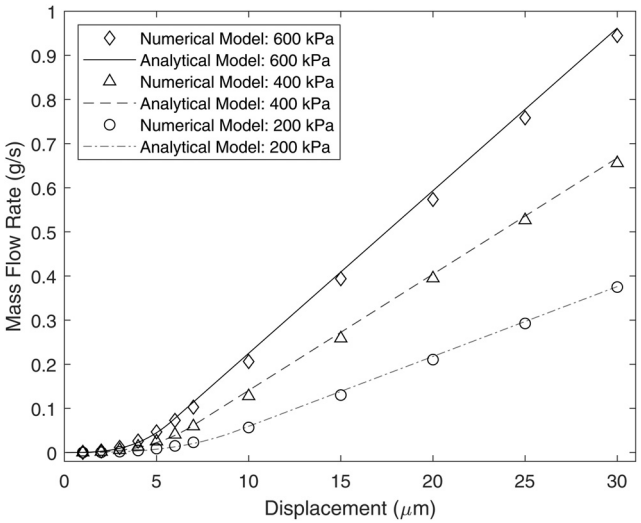

Fig. 12 Numerical flowrate through etched metallic seal with seal boss $t_s = 800\ \mu$m plotted against analytical model. Pressures shown are gauge pressures.

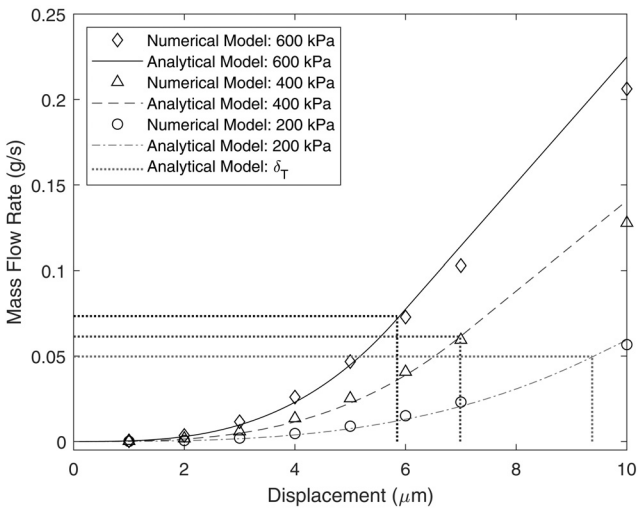

Fig. 13 Numerical flowrate with seal boss $t_s = 800\ \mu$m plotted against analytical model with flowrate at δ_T identified. Pressures shown are gauge pressures.

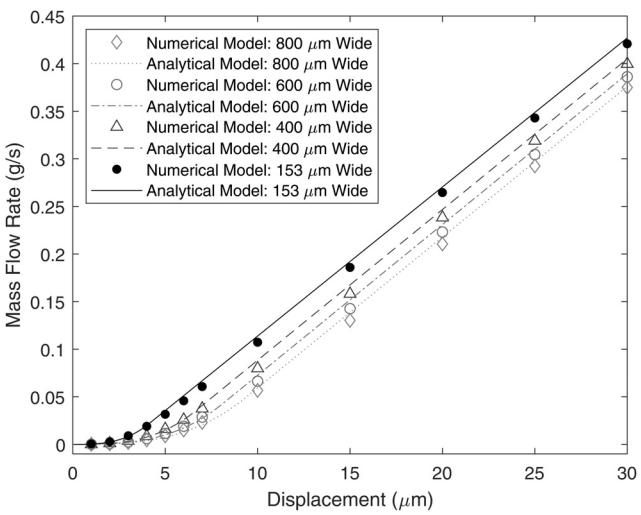

Fig. 14 Numerical flowrate with varying seal boss t_s of 153, 400, 600, and 800 μm plotted against analytical model at 200-kPa gauge inlet pressure. Pressures shown are gauge pressures.

Table 1 δ_T for the seal plate designs at the pressures tested

P_1 (kPa)	t_s (μm)	δ_T (μm)	$\dot{m}_{\delta_T}$ (g/s)	P_1 (kPa)	t_s (μm)	δ_T (μm)	$\dot{m}_{\delta_T}$ (g/s)
200	150	4.10	0.031	400	600	6.02	0.052
200	400	6.59	0.033	400	800	6.95	0.059
200	600	8.08	0.041	600	150	2.56	0.022
200	800	9.33	0.048	600	400	4.11	0.050
400	150	3.06	0.027	600	600	5.04	0.060
400	400	4.92	0.042	600	800	5.82	0.070

significant impact on the length of the nonlinear microchannel flow regime.

Mass flowrate versus displacement for varying seal boss widths at an inlet pressure of 200-kPa gauge is shown in Fig. 14. The slope of the seal-limited flow regime is constant for all seal boss widths, signifying that the seal boss width has minimal to no impact on flow efficiency in the seal-limited flow regime. However, δ_T has a strong dependency on the seal boss width with increasing values of t_s leading to larger values of δ_T.

The relationship between δ_T, P_1, and t_s from numerical simulations is shown in Table 1. At lower pressures, t_s has a larger impact on mass flowrate than at larger pressures. As inertial forces increase at higher pressures, t_s has a smaller impact on δ_T. Observed changes in flow capacity at a given pressure are due largely to varying δ_T, attributed to changes in seal boss width. The larger the value of δ_T, the lower the overall flow capacity of the valve seal design.

5 Experiments

The experiments were intended to validate data created with the analytical and numerical models using similar geometry. Experimental variation of seal plate parameters was limited due to limitations of the PCE process. For example, radial seal width t_s could not be reduced below 150 μm using a 305-μm thick seal plate because doing so resulted in a discontinuous seal. Similarly, study of the impact of seal boss height on flow regime was only possible through numerical modeling, as a constant seal plate thickness was used throughout this study, and the etching process required h_s to be equal to h_p (see Fig. 2).

The experimental apparatus for testing the prototype (illustrated in Fig. 3) is described below. An experiment to measure actual flow versus displacement is reviewed next. An experiment exploring leak rate is then described.

5.1 Valve Seal Characterization Test Bench. The test bench for the hardware prototype valve was designed according to the ISO 6358:1989 standard [24]. It consisted of an upstream 10-μm air filter, an upstream pressure regulator, and a series of upstream sensors, as shown schematically in Fig. 15. The sensors included: a mass flowmeter to measure mass flowrate, $\dot{m}$, an upstream pressure sensor to measure stagnation pressure, P_0, and an upstream temperature sensor to measure stagnation temperature, T_0. Sensor data were collected using a data acquisition system.

A linear variable differential transformer (LVDT)[5] was paired with a needle-type end effector at the outlet of the valve to gather real-time displacement data on the seal plate position. The LVDT was mounted to the bottom of the valve with a simple cage fixture. Each data point was taken discretely at the desired displacement, and then the seal was returned to $\delta = 0\ \mu$m.[6] Flow moved through the valve seal assembly as shown in Fig. 3(*b*).

5.2 Flow Rate Versus Displacement: Experimental. All components shown in Fig. 3(*a*) were installed for the flowrate

[5]Keyence High Precision GT2-UB1 LVDT.

[6]Data points were take discretely to minimize impact of needle probe thermal expansion on displacement measurement accuracy.

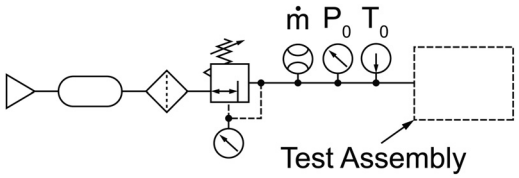

Fig. 15 Flow characterization test stand system schematic

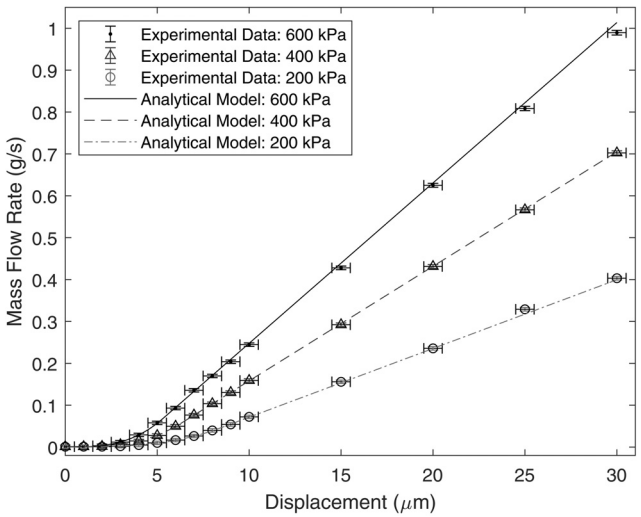

Fig. 16 Experimental full displacement range flowrate data through etched metallic seal with seal boss $t_s = 654\ \mu$m plotted against analytical model. Pressures shown are gauge pressures.

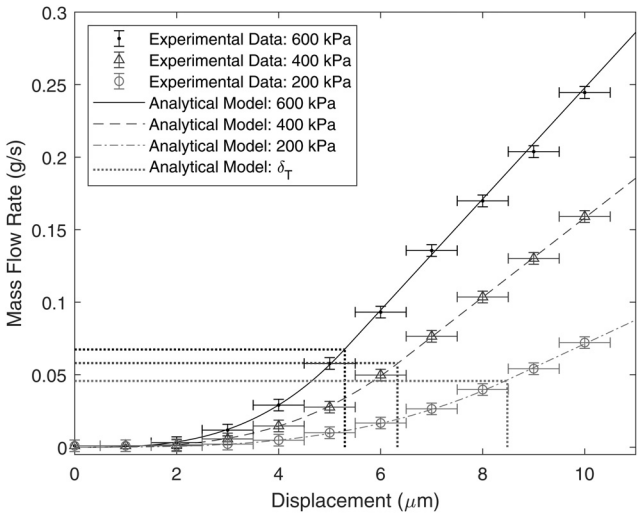

Fig. 17 Close-up view of the low-displacement region of Fig. 12. Pressures shown are gauge pressures. The transition displacements are $\delta_T(200\,\text{kPa}) = 8.45\ \mu m$, $\delta_T(400\,\text{kPa}) = 6.30\ \mu m$, and $\delta_T(600\,\text{kPa}) = 5.27\ \mu m$.

experiments. The carrier, control rods, and rod mount were rigidly connected via a two-part epoxy.[7] PCE process variability led to a small difference between experimental and numerical model geometry for D_s (experimental $D_s = 7.90$ mm, and numerical

[7]3M DP420.

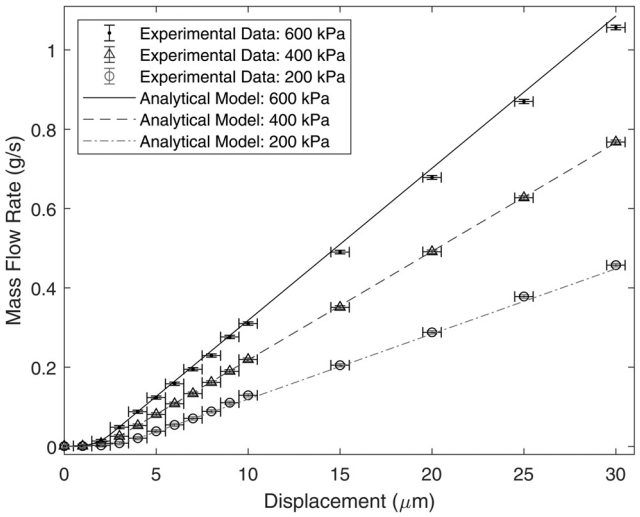

Fig. 18 Experimental full displacement range flowrate data through etched metallic seal with seal boss $t_s = 153\ \mu$m plotted against analytical model. Pressures shown are gauge pressures.

$D_s = 7.80$ mm). Outlet pressure was experimentally measured to be 99 kPa.

Flow versus displacement experiments were performed for two seal boss widths. Results for a 654-μm wide seal boss are shown in Figs. 16 and 17. Results for a 153-μm wide seal boss are shown in Fig. 18.

Discharge coefficient C_D was determined for each seal boss width tested by applying Eq. (11) to the data points in the seal-limited flow regions for each of three test pressures, then averaging the three resulting C_D values. The C_D values calculated for $t_S = 654\ \mu$m and $t_S = 153\ \mu$m were consistent: 0.935 and 0.937, respectively.

It is noted that the C_D values used for the experiments differ slightly from those used for the numerical studies (0.91). The difference is likely attributable to the inability of the numerical model to capture all physical details of the actual flow passages, such as corner radii on the seal bosses and surface finish.

The piecewise analytical model matches experimental data closely in both the microchannel and seal-limited flow regimes. Experimental error depicted by the error bars accounted for both accuracy of displacement measurement and accuracy of flowrate measurement. The displacement measurement error was attributed

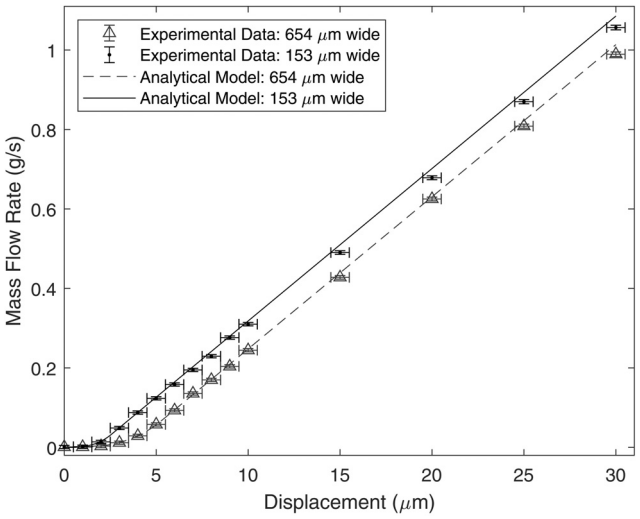

Fig. 19 Experimental flowrate data through an etched metallic seal with seal boss $t_s = 153\ \mu$m and $t_s = 654\ \mu$m plotted against analytical model at a 600-kPa gauge inlet pressure

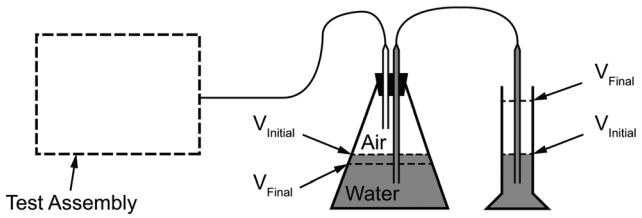

Fig. 20 Leak test flow measurement apparatus

to the measurement accuracy of the LVDT and also repeatability error. The summed displacement error was $\pm 0.5\ \mu$m. The flowrate measurement error was attributed solely to the accuracy of the 100 SLPM capacity mass flowmeter used for this test case.[8] This error was ± 0.004 g/s.

The seal boss width has significant impact on flow versus displacement curve shape and flow capacity. Figure 19 shows a comparison of experimental and piecewise analytical model data for seal plates with seal boss widths of $t_s = 153\ \mu$m and $t_s = 654\ \mu$m at 600-kPa gauge inlet pressure. Analysis of these data reveals that a wider seal boss will lead to a longer region of nonlinear flow in the microchannel regime.[9] This reduces overall flow capacity.

5.3 Leak Rate Study. Leak rate as a function of seal plate design was studied solely by experiment. Only the components shown in Fig. 3(*b*) were installed for the leak tests, e.g., the piezostack was not included. The seal plate spring applied a prescribed preload between the seal plate and the orifice plate while maintaining parallelism between the two mating surfaces.

Two samples of a 153-μm wide seal boss and three samples of a 654-μm wide seal boss were tested. The preload pressure on the 153-μm seal boss was estimated to be 2837 kPa, while the preload pressure on the 654-μm seal boss was estimated to be 625 kPa. Seal plate design parameters held constant in the leak test case were: $h_s = 152.5\ \mu$m, $D_s = 7.90$ mm, and $D_o = 2.78$ mm. The outlet was venting to atmospheric pressure, measured to be 99 kPa.

Leaks were measured using a 1 SLPM capacity mass flowmeter.[10] However, some leaks were so small that they could not be measured accurately with the stock device. Therefore, an additional flow measurement apparatus was used to calibrate the 1 SLPM mass flowmeter at very low mass flow rates. The apparatus is shown schematically in Fig. 20.

Air exiting the test assembly was routed into a sealed volumetric flask filled with known volumes of air and water. A primed water line was routed between the sealed volumetric flask and a graduated cylinder open to the air. Air entering into the sealed volumetric flask produced a change in water volume in the graduated cylinder. Figure 20 illustrates water levels before and after a test as V_{Initial} and V_{Final}, respectively. This change in water volume was divided by elapsed testing time to quantify leak rate through the seal assembly. Use of the additional measurement apparatus enabled accurate leak testing down to flow rates of 3×10^{-3} mg/s with an uncertainty of $\pm 12\%$ of the measured value.

The leak rate for each seal assembly sample is plotted against the inlet pressure in Fig. 21. The experimental data are plotted with error bars describing the $\pm 12\%$ flowrate measurement uncertainty described above.

Analysis of the results yielded two conclusions. First, the metallic seals had very small leak rates and would be suitable to applications requiring low leak rates. For example, at a 600-kPa gauge inlet pressure, the worst-performing seal assembly having a 654-μm wide seal boss had a mass flowrate of 6.1×10^{-5} g/s. This would result in a turndown ratio of around 16,000, which is exceptionally good. The

[8]Alicat M-Series 100 SLPM capacity.
[9]The effect of seal boss width on sealing is discussed further in Sec. 5.3.
[10]Alicat M-Series 1 SLPM capacity.

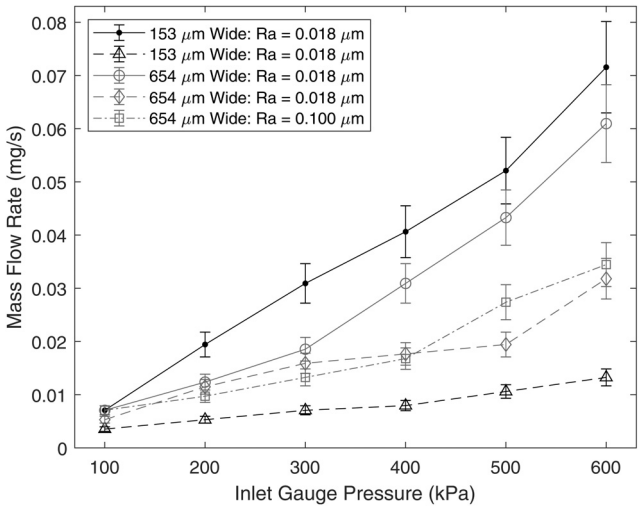

Fig. 21 Experimental leak rate through etched metallic seals with seal bosses of widths 153 μm and 654 μm

seal assembly with the lowest leak rate at the same pressure reported a value of 1.3×10^{-5} g/s.

Second, the leak rate of the tested seal assemblies showed no strong correlation with either the seal boss width[11] or the average surface roughness. To understand the second conclusion, it is useful to draw analogy to Eq. (1). While direct comparison between Eq. (1) and the leak rate results was not practical, relevant dimensions of interest could still be inferred

$$\dot{m}_{\text{Leak}} \propto [\delta_{\text{Avg}}]^3 [D_s]^1 [t_s]^{-1} \tag{14}$$

where δ_{Avg} is the average gap between the seal plate and the orifice plate, the primary contributor to leakage.

δ_{Avg} is a function of average surface roughness, local seat flatness, and global seat flatness. Optical measurement of average surface roughness and local flatness was completed for the tested samples.[12] Samples were very smooth with roughness average measurements of 0.018 μm for samples with a mirror finish and 0.100 μm for a sample without. Local flatness measurements were of the order of 2.5 μm, but varied depending on measurement trace location. Global flatness measurements were not attempted as the leak testing would act to flatten the seal assembly samples with increasing seal pressures.

The experiments indicate that average roughness and seal assembly geometry were not significant factors in predicting leak rate. The flatness of the seal assembly was likely the primary contributor to δ_{Avg}. More comprehensive study of leak rates at the tested conditions would require addition of a sealing pressure-based parameter to assess δ_{Avg} as a function of material deformation, as described by Marie and Lasseux [6].

6 Discussion

Figures 1, 6, 8, 12–14, and 16–19 demonstrate that Eq. (10) is capable of accurately representing flow through a valve that has a substantial portion of its travel in both the microchannel and seal limited flow regimes. In this section, the reasonableness of disregarding the Knutson term in Eq. (1) is explored, then the new model is compared with existing models.

Flow behavior for low displacements of the seal plate with a 654 μm wide seal boss is illustrated in Fig. 17.[13] The resolution of the

[11]This is in contrast to the numerical study of Sec. 4.2, where leak rate decreased with increasing seal boss width.
[12]Optical measurements used a trace length of 1.27 mm.
[13]The 654 μm wide seal boss is explored here because it remains in the microchannel flow regime longer than the 153 μm wide seal boss.

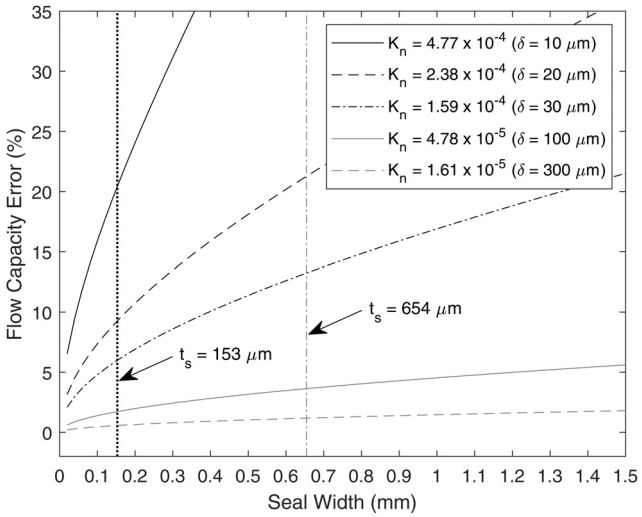

Fig. 22 Mass flowrate prediction error by linear analytical flow models [9,13] in comparison to the presented piecewise analytical flow model

mass flowmeter used in the experiments is not sufficient to precisely quantify what is happening for displacements below 2 μm, where the Knutson term would have greatest impact. However, good agreement between the analytical model and all experimental data indicate that Eq. (10) captures the overall valve performance well, regardless of disregarding the Knutson term, for valves having displacement ranges that move into the seal limited flow regime.

Some existing models utilize a linear orifice flow based model from $\delta = 0$ μm until flow reaches a transition regime between the seal limited and orifice limited regimes [9,13]. Other existing models utilize a microchannel model. While various derivations of the microchannel model exist, all include a cubic dependence on δ [5,20]. Figure 1 compares the linear, the cubic, and the new piecewise analytical model. Clearly, the piecewise analytical model is required to correctly predict the flowrate in a valve where the seal design moves between the microchannel and seal limited flow regimes.

Many flow conditions and seal designs exist where conventional linear analytical models may incorrectly predict flow rates. For example, Fig. 22 illustrates the differences between the existing linear and the new piecewise analytical models at six displacements at an inlet pressure of 600-kPa gauge while venting to atmosphere.

Increases in seal width or K_n, or decreases in δ, led to increased calculated error of flow capacity. The modeled flow capacity error was significant for both the prototype valve and valves with differing design parameters. For example, in a valve with a seal width of 654 μm, a seal boss inner diameter of 7.8 mm, and an actuator displacement of 30 μm, use of the linear model would result in a 13.3% error in predicted flow capacity. For the same valve using an actuator with a 300-μm displacement, the linear model yields only a 1.2% error. At lower inlet pressures such as 200-kPa gauge, the error becomes even more significant with 23.2% error at 30 μm of displacement and 1.9% error at 300 μm of displacement. This simple comparison illustrates that existing linear analytical models are not adequate for top-down design of pneumatic valves with small displacements.

A minor limitation of Eq. (10) is that it is only valid when the pressure differential across the valve is sufficient to cause the flow to choke in the seal limited flow regime. Fortunately, the majority of applications are likely to fall into this range. Nevertheless, extending the piecewise model to cover situations where flow is subsonic in the seal limited flow regime would comprise a desirable future enhancement.

7 Conclusion

An efficient etched metallic valve seal featuring a cylindrically shaped boss was designed and studied. The focus of this work is to introduce and validate an analytical method for modeling compressible flow through a valve seal having this design. The model combines an existing microchannel flow model with the well-known orifice theory-based flow model to accurately describe flow through the valve for any seal displacement in its overall range. The model is validated both numerically and experimentally.

The studies revealed that well-lapped etched seal plates were capable of leak rates as low as 1.3×10^{-5} g/s and flow rates as high as 1.057 g/s at 600 kPa with a seal displacement of only 30 μm. Study of the impact of seal boss width on flowrate characteristics indicated that increases in seal width provided both slightly reduced flow capacity and linear range. While the numerical studies indicated that sealing should improve with increasing seal width, experimental studies indicated that seal flatness was the dominant parameter in determining sealing. The results will enable engineers to better perform model based design of valves using small displacement actuators and flat valve seals.

Acknowledgment

The authors thank the National Fluid Power Association Education and Technology Foundation for a Research Supplement Award.

Funding Data

- National Science Foundation (Grant Nos. PFI-2016330 and I-CORPS-1940068; Funder ID: 10.13039/100000001).

Data Availability Statement

The datasets generated and supporting the findings of this article are obtainable from the corresponding author upon reasonable request.

References

[1] Oh, K. W., and Ahn, C. H., 2006, "A Review of Microvalves," J. Micromech. Microeng., **16**(5), pp. R13–R39.
[2] Smal, O., Raucent, B., and Jeanmart, H., 2009, "Fluid Flow Modelling of a Micro-Valve," Int. J. Simul. Multidiscip. Des. Optim., **3**(2), pp. 356–362.
[3] Smal, O., Raucent, B., Ceyssens, F., Puers, R., De Volder, M., and Reynaerts, D., 2008, "Design and Testing of an Ortho-Planar Micro-Valve," Confirmation of Large-Periphery Compressible Gas Flow Model for Microvalves, Vol. 4, *4th International Precision Assembly Seminar*, Chamonix, France, Feb. 10–13, pp. 75–86.
[4] Lynch, B. A., Jamieson, B. G., Roman, P. A., and Zakrzwski, C. M., 2005, "An Empirical Study of Boss/Seat Materials and Geometries for Ultra Low-Leakage MEMS Micro-Valves," ASME Paper No. IMECE2005-81082.
[5] Park, J. M., Evans, A. T., Rasmussen, K., Brosten, T. R., Nellis, G. F., Klein, S. A., and Gianchandani, Y. B., 2009, "A Microvalve With Integrated Sensors and Customizable Normal State for Low-Temperature Operation," J. Microelectromech. Syst., **18**(4), pp. 868–877.
[6] Marie, C., and Lasseux, D., 2007, "Experimental Leak-Rate Measurement Through a Static Metal Seal," ASME J. Fluids Eng., **129**(6), pp. 799–805.
[7] Johnson, C., Khodadadi, J., and Yang, E., 2006, "Modeling of Frictional Gas Flow Effects in a Piezoelectrically Actuated Low Leak-Rate Microvalve Under High-Pressure Conditions," J. Micromech. Microeng., **16**(12), pp. 2771–2782.
[8] Tang, W., Chakraborty, I., and Pyle, D., 1998, "Deep Reactive-Ion Etched Micro Valves for Spacecraft Propulsion," Version V1, Jet Propulsion Laboratory, https://hdl.handle.net/2014/20661.
[9] van der Wijngaart, W., Thorsen, A., and Stemme, G., 2005, "A Seat Microvalve Nozzle for Optimal Gas-Flow Capacity at Large-Controlled Pressure," J. Microelectromech. Syst., **14**(2), pp. 200–206.
[10] Gradin, H., Braun, S., Stemme, G., and van der Wijngaart, W., 2012, "SMA Microvalves for Very Large Gas Flow Control Manufactured Using Wafer-Level Eutectic Bonding," IEEE Trans. Ind. Electron., **59**(12), pp. 4895–4906.
[11] Pan, C.-P., and Wang, D.-H., 2016, "Modeling and Experimental Verification of the Flow Characteristics of an Active Controlled Microfluidic Valve With Annular Boundary," J. Intell. Mater. Syst. Struct., **27**(16), pp. 2237–2248.
[12] White, F. M., 2008, *Fluid Mechanics*, 6th ed., McGraw-Hill, Boston, MA, pp. 617–618.
[13] Henning, A. K., 2004, "Confirmation of Large-Periphery Compressible Gas Flow Model for Microvalves," MEMS/MOEMS Components and Their Applications, Vol. 5344, International Society for Optics and Photonics, San Jose, CA, Jan. 26–27, pp. 155–162.

[14] Henning, A. K., 2003, "Improved Gas Flow Model for Microvalves," 12th International Conference on Solid-State Sensors, Actuators and Microsystems (TRANSDUCERS 03), Boston, MA, June 8–12, pp. 1550–1553.
[15] Henning, A. K., 2000, "Compact Pressure-and Structure-Based Gas Flow Model for Microvalves," Materials and Device Characterization in Micromachining III, Vol. 4175, International Society for Optics and Photonics, Santa Clara, CA, Sep. 18–19, pp. 74–81.
[16] Arkilic, E. B., Schmidt, M. A., and Breuer, K. S., 1997, "Gaseous Slip Flow in Long Microchannels," J. Microelectromech. Syst., **6**(2), pp. 167–178.
[17] Agrawal, A., 2011, "A Comprehensive Review on Gas Flow in Microchannels," Int. J. Micro-Nano Scale Transp., **2**(1), pp. 1–40.
[18] Cavazzuti, M., Corticelli, M. A., and Karayiannis, T. G., 2019, "Compressible Fanno Flows in Micro-Channels: An Enhanced Quasi-2D Numerical Model for Laminar Flows," Therm. Sci. Eng. Prog., **10**, pp. 10–26.
[19] Asako, Y., Pi, T., Turner, S. E., and Faghri, M., 2003, "Effect of Compressibility on Gaseous Flows in Micro-Channels," Int. J. Heat Mass Transfer, **46**(16), pp. 3041–3050.
[20] Fazal, I., and Elwenspoek, M. C., 2007, "Design and Analysis of a High Pressure Piezoelectric Actuated Microvalve," J. Micromech. Microeng., **17**(11), pp. 2366–2379.
[21] Barber, R., and Emerson, D., 2002, "The Influence of Knudsen Number on the Hydrodynamic Development Length Within Parallel Plate Micro-Channels," Advances in Fluid Mechanics IV, 4th International Conference on Advances in Fluid Mechanics, Ghent, Belgium, May, pp. 207–216.
[22] Menter, F. R., Langtry, R. B., Likki, S. R., Suzen, Y. B., Huang, P. G., and Völker, S., 2006, "A Correlation-Based Transition Model Using Local Variables-Part I: Model Formulation," ASME J. Turbomach., **128**(3), pp. 413–422.
[23] Evgenevna, I. E., Evgenevna, I. T., and Viktorovich, B. P., 2014, "Analysis of the Application of Turbulence Models in the Calculation of Supersonic Gas Jet," Am. J. Appl. Sci., **11**(11), pp. 1914–1920.
[24] ISO 6358:1989(E), 1989, *Pneumatic Fluid Power - Components Using Compressible Fluids - Determination of Flow-Rate Characteristics*, International Organization for Standardization, Geneva, CH.